

Monitoring of wind turbine blades for flutter instability

Bei Chen^{*1}, Xu G. Hua^{1a}, Zi L. Zhang^{2b}, Biswajit Basu^{3c} and Søren R.K. Nielsen^{4d}

¹Key Laboratory for Wind and Bridge Engineering, Department of Civil Engineering, Hunan University, Changsha 410082, China

²Department of Engineering, Aarhus University, Aarhus 8000, Denmark

³School of Engineering, Trinity College Dublin 2, Ireland

⁴Department of Civil Engineering, Aalborg University, Aalborg 9000, Denmark

(Received February 16, 2017, Revised June 7, 2017, Accepted June 8, 2017)

Abstract. Classical flutter of wind turbine blades indicates a type of aeroelastic instability with fully attached boundary layer where a torsional blade mode couples to a flapwise bending mode, resulting in a mutual rapid growth of the amplitudes. In this paper the monitoring problem of onset of flutter is investigated from a detection point of view. The criterion is stated in terms of the exceeding of a defined envelope process of a specific maximum torsional vibration threshold. At a certain instant of time, a limited part of the previously measured torsional vibration signal at the tip of blade is decomposed through the Empirical Mode Decomposition (EMD) method, and the 1st Intrinsic Mode Function (IMF) is assumed to represent the response in the flutter mode. Next, an envelope time series of the indicated modal response is obtained in terms of a Hilbert transform. Finally, a flutter onset criterion is proposed, based on the indicated envelope process. The proposed online flutter monitoring method provided a practical and direct way to detect onset of flutter during operation. The algorithm has been illustrated by a 907-DOFs aeroelastic model for wind turbines, where the tower and the drive train is modelled by 7 DOFs, and each blade by means of 50 3-D Bernoulli-Euler beam elements.

Keywords: wind turbine; flutter monitoring; envelope process; Hilbert-Huang transform

1. Introduction

Flutter in wind turbine blades is caused by an unfavorable interaction of aeroelastic, elastic and inertial forces, which may lead to major structural failure of the blades. In a steady homogeneous wind field the onset of flutter takes place, if the average power absorbed by the structure from the self-induced loads exceeds the average power dissipated by the structural damping and other active or passive damping mechanism mounted on the structure. Classical flutter of a beam-like structure such as wind turbine blades is explained as an unfavourable aerodynamic coupling between flapwise and torsional vibrations of the blades, and appears in a rapid growth of the amplitudes of

*Corresponding author, Ph.D. Candidate, E-mail: chamber@hnu.edu.cn

^a Professor, Email: cexghua@hotmail.com

^b Ph.D., Email: zili_zhang@eng.au.dk

^c Professor, Email: basub@tcd.ie

^d Professor, Email: srkn@civil.aau.dk

the flapwise and torsional motions Politakis (2008), Zhang (2011), Hayat (2016).

An early example of classical wind turbine flutter has been investigated in a laboratory test with a scaled Vertical Axis Wind Turbine (VAWT) model, Popelka (1982). For small Horizontal Axis Wind Turbines (HAWT) the critical rotational speed for flutter Ω_{cr} is known to be significantly higher than the nominal rotor speed Ω . The critical rotational speed for flutter of a 20 KW HAWT with a rotor diameter of 5 m were found to be approximately six times the nominal rotor speed, Lobitz *et al.* (1998). For a 1.5 MW WindPACT wind turbines, the critical rotational speed for flutter is about twice the nominal rotor speed, Lobitz (2004). Such wind turbines do not experience flutter due to their high torsional angular frequency in comparison to the angular eigenfrequency in the critical flapwise bending mode of the blades. Further, studies also show that it was the second flapwise mode and the first torsional blade mode which coupled into flutter, Lobitz (2004), Hansen (2004). Similar result has also been found for a 5 MW NREL turbine. In this case it was shown the third flapwise mode that coupled with the first torsional blade mode, Bir (2007), Hansen (2007). Vatne (2011) showed that the critical rotational speed for flutter is found to be about 1.6 times the nominal rotor speed for a 10 MW NOWITECH wind turbine. Even though classical flutter has not been observed on modern full scale pitch-regulated wind turbines, it is believed that with further increase of the magnitude of wind turbines, flutter will become a more important design consideration, Zhang (2011). Actually, study on enhancing flutter stability of wind turbine blade has been discussed in detail by author in Bei (2016).

Several studies have been carried out on the stability analysis, especially for the flutter of wind turbine blade. Bir (2007) proposed a Multi-blade coordinate transformation (MBC, Johnson (1980)) eigenvalue analysis. This approach involves a linearization of the structural equations of motion, the aerodynamic loads, the pitch and generator control laws about a steady-state equilibrium, Hansen (2007, 2004). If the nominal rotational speed of the rotor is assumed to be constant in time at the nominal value, this approach results in linear equations of motion with periodical varying terms in the system matrixes. Alternatively, the aeroelastic stability may be alternatively checked by a Floquet analysis on the nontransformed linearized equations, Nayfeh (1995), Tcherniak (2016).

For the flutter monitoring studies, most works are offline and mostly are focused on aircrafts. little study has been carried out for online monitoring for the onset of flutter, especially for wind turbine blades. Mevel proposed a series of online statistical subspacebased methods for flutter monitoring of aircrafts. Each method evaluating a predefined stability criterion in terms of damping coefficient or flutter margin. Studies by Mevel (2005) show an online detection method for the onset of flutter of aircraft wing by monitoring the damping coefficient. Based on the state observer and Subspace Identification (SI), they defined a residual vector, which reflects the characteristics of damping coefficient. By using the online cumulative sum (CUSUM), the variation of the damping coefficient can be reflected through a statistical parameter. Their criterion for the onset of flutter is defined such that the damping coefficient decreases below some specified critical value. Similar studies has also been carried out by Zouari (2012). Based on the Subspace Identification method Zhou (2007) used an new parameter, the so called flutter margin basically indicating the numerical difference between two complex eigenvalues, to represents the interaction between the bending and torsional mode, which indicates the onset of flutter.

From authors' point of view, the stability analysis may also be performed by observing a certain envelope of the flapwise or torsional motions, indicating the evolution with time of the amplitude of the involved response quantities. Hence, flutter is defined to take place when the envelope of the torsional angle exceeds a certain critical value θ_m . In this paper a monitoring technique for the

onset of flutter of wind turbine blades is described. Firstly, the original torsional vibration time series of the blade tip is decomposed into n th Intrinsic Mode Functions (IMFs) through Empirical Mode Decomposition (EMD). Then, the 1st IMF, which represents the flutter mode, is chosen to calculate the envelope process through the Hilbert Transform. Finally, a flutter onset criterion is proposed based on that envelope process. This approach is more practical and useful if the instability is dominated by nonlinear mechanisms, either structural or aeroelastic.

2. Modelling of flutter induced vibrations of wind turbines

In this section, a 907-DOF aeroelastic wind turbine model is presented. This model takes several important characteristics of a wind turbine into account, including time dependent system matrices, coupling of the tower-blades-drive-train vibration as well as nonlinear aeroelasticity. Further, the aeroelastic load is described in detail.

2.1 Wind turbine model

Fig. 1 shows a schematic representation of the wind turbine model with definitions of the coordinate systems and the degrees of freedom of tower. As seen, the motion of the tower is described in a fixed, global (X_1, X_2, X_3) -coordinate system with a origin O at the interface to the foundation. Further, the motion of each blade is described in a moving, local (x_1, x_2, x_3) -coordinate system with origin O' at the center of the hub. Neglecting the tilt and cone of the rotor, the X_1 - and x_1 -axis are unidirectional parallel to the mean wind velocity direction. (x_2, x_3) and (X_2, X_3) coordinate planes are placed in the rotor plane and is parallel to each other. The x_3 - axis is placed along the undeformed blade axis oriented from the hub towards the blade tip and the X_3 -axis is vertical. Then, the position of the local coordinate system attached to blade j is merely specified by the azimuthal angle $\Psi_j(t)$ which is considered positive when rotating clockwise seen from an upwind position.

The motion of tower is defined by the translational degrees of freedom $q_1(t)$ and $q_2(t)$ in the global X_1 - and X_2 -directions, and the rotational degrees of freedom $q_3(t)$, $q_4(t)$, $q_5(t)$ in the global X_1 - and X_2 -directions. $q_3(t)$ is considered positive in the negative X_1 -direction, and $q_4(t)$ and $q_5(t)$ in the positive X_2 - and X_3 -directions.

L denotes the length of the blade from the hub to the blade tip. the height of the tower from the base to the nacelle is denoted by h , and the horizontal distance from the center of the tower top to the origin O' of the moving coordinate systems is denoted s .

The tower is modelled as a Euler-Bernoulli beam fixed at the tower support, infinitely rigid against external deformations, and with variable mass per unit length and variable bending stiffness.

The drive-train is modeled by the degrees of freedom $q_6(t)$ and $q_7(t)$ as shown in Fig. 2, indicating elastic deformation (the rotational angle of the rotor and the generator rotor), respectively. $M_r(t)$ and $M_g(t)$ denote the work-conjugated rotor torque and generator torque. The gear wheels are considered rigid, and all flexibility is confined to the rotor and generator shafts. The sign definition shown in Fig. 2 applies to a gearbox with odd number of stages. In case of even number of stages the sign definitions for $q_7(t)$ and $M_g(t)$ are considered positive in the opposite direction.

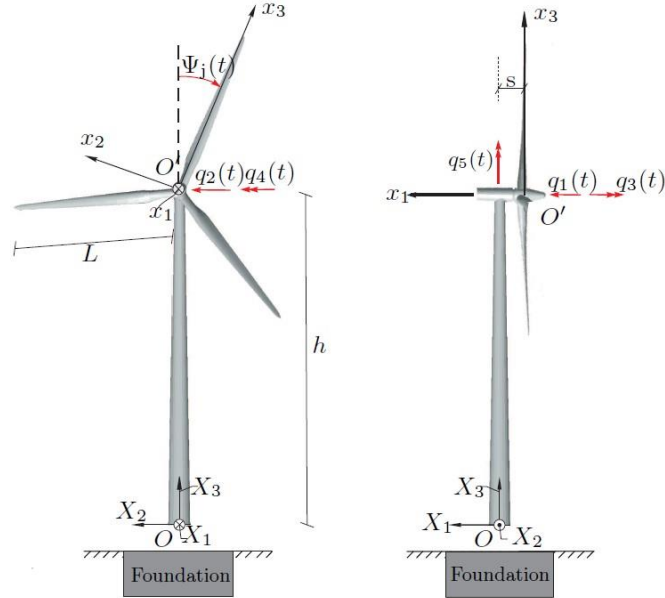


Fig. 1 Definition of the fixed and the moving frames of reference and the degrees of freedom $q_1(t), \dots, q_5(t)$

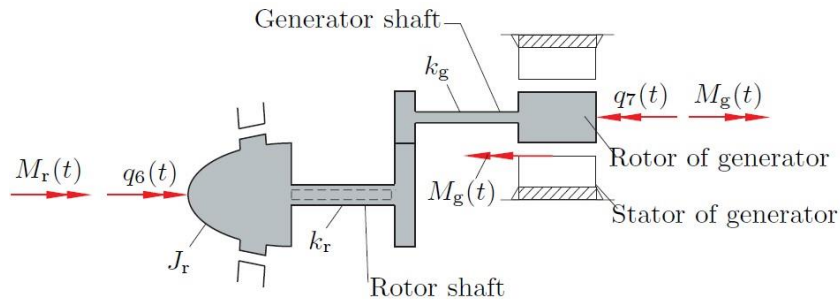


Fig. 2 2-DOF model of flexible drive train with odd number of gear stages. Definition of degrees of freedom $q_6(t)$, and $q_7(t)$

J_r and J_g are the mass moment of inertia of the rotor and the generator, respectively. k_r and k_g denote the St.Venant torsional stiffness of the rotor and generator shafts. The degrees of freedom $q_1(t), \dots, q_7(t)$, which specified the motion of the tower and the drive train, are assembled in the column vector $\mathbf{q}_0(t)$. The kinetic and strain energy of the tower and the drive train minus the rotor can be calculated on the basis of $\mathbf{q}_0(t)$ and $\dot{\mathbf{q}}_0(t)$. The kinetic energy related to the rotor is accounted for at the analysis of the blades.

The rotation of each blade is assumed to take place with a constant nominal rotational speed Ω . Then, the azimuthal angle $\Psi_j(t)$ for blade j may be given as

$$\Psi_j(t) = \Omega t + q_6(t) + \frac{2\pi}{3}(j - 1) \approx \Omega t + \frac{2\pi}{3}(j - 1) \quad , \quad j = 1, 2, 3 \quad (1)$$

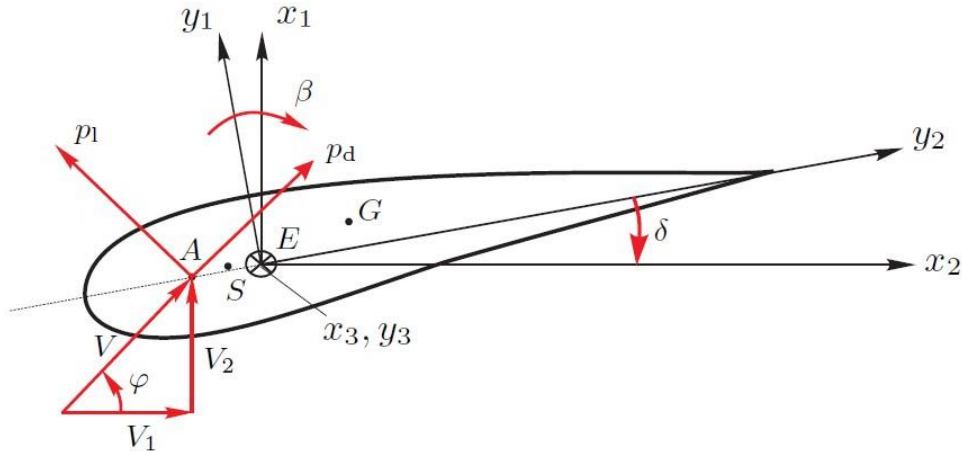


Fig. 3 Definition of principal axis coordinate system

where $\Psi_j(t)$ denotes the azimuthal angle of blade $j = 1, 2, 3$, Ω indicates the nominal rotational speed of the rotor. $q_6(t)$ is a degree of freedom specifying the deviatoric rotation of the hub on top of the nominal rotational angle Ωt . Since $q_6(t)$ is a numerically small quantities compared to Ωt , $q_6(t)$ can be ignored in Eq. (1).

Each blades is modeled as a Bernoulli-Euler beam with variable mass per unit length $\mu(x_3)$ and variable bending stiffness in the flapwise and edgewise directions. Deformations from the shear forces are ignored. The elastic center E of all cross-sections along the blade are assumed to be placed along the x_3 -axis. For each cross section a principal axis (y_1, y_2, y_3)- coordinate is defined as shown in Fig. 3. The y_3 -axis is unidirectional and parallel to the x_3 -axis. The orientation of the y_2 -axis is decided by the angle $\delta(x_3)$, indicating the angle from the y_2 -axis into the x_2 -axis in the positive x_3 -direction. $\delta(x_3)$ indicates the pretwist of the blade section. Fig. 3 also shows the aerodynamic center A , the shear center S and the mass center G . The position of the aerodynamic center A is assumed to be fixed with time. In order to decouple the equations of motion for the elastic torsion and bending displacement, the external aerodynamic lift force per unit length p_l and drag force per unit length p_d acting in the aerodynamic center is transferred to the shear center when formulated in the (y_1, y_2, y_3)- coordinate system. The inertial loads, including the gravity load, are acting in the mass center G . The gravity loads are referred to the shear center for the same reason as for the aerodynamic loads. The components of velocity vector and angular velocity vector of the mass center need to be interpolated from the time derivatives of the degrees-of-freedom of the element. Hence, the kinetic energy, the mass matrix, the gyroscopic damping and stiffness matrices of the element can be calculated based on the above interpolation functions. However, the inertial loads are actually acting in the mass center G and not in the elastic center E , which will introduces couplings in the equation of motion of importance for the flutter stability.

Fig. 4 illustrates that a blade has been divided into n th elements, including the global node numbering. $x_{3,j}$ indicates the position of node j of the element along the x_3 -axis. Also shown is the length of beam element j between the nodes j and $j + 1$ and the definitions of the twelve

degrees of freedom $r_{1,j}, \dots, r_{12,j}$ in the principal axis coordinate system of each beam element. $l_j = x_{3,j+1} - x_{3,j}$ indicates the element length. The degrees-of-freedom specifying the elastic deformation of blade j relative to the hub in the local (x_1, x_2, x_3) -coordinate system, are assembled in the column vector $\mathbf{q}_j(t)$, $j = 1, 2, 3$ of dimension $6n$. Based on the small elastic vibrations assumption, linear beam theory may be assumed with due consideration of the geometrical stiffening in the x_3 -direction, and the geometrical softening in transverse direction. The specific expression of the displacement and velocity vector of the blades can be found in Zhang (2014).

The degrees of freedom of the system are assemble in the column vectors $\mathbf{q}(t)$ of dimension $7 + 18n$

$$\mathbf{q}(t) = \begin{bmatrix} \mathbf{q}_0(t) \\ \mathbf{q}_1(t) \\ \mathbf{q}_2(t) \\ \mathbf{q}_3(t) \end{bmatrix} \quad (2)$$

The kinetic energy $T(\mathbf{q}, \dot{\mathbf{q}})$ and the potential energy $U(\mathbf{q})$ of the tower, drive train and blades may be calculated as a function of $\mathbf{q}(t)$ and $\dot{\mathbf{q}}(t)$ based on the discretization of the blades. Then, the equations of motion of the tower, the drive train and the blades follow from the Euler-Lagrange stationarity condition of analytical dynamics, Lurie (2013), Hsu (2014)

$$\frac{d}{dt} \left(\frac{\partial T(\mathbf{q}, \dot{\mathbf{q}})}{\partial \dot{\mathbf{q}}} \right) - \frac{\partial T(\mathbf{q}, \dot{\mathbf{q}})}{\partial \mathbf{q}} + \frac{\partial U(\mathbf{q})}{\partial \mathbf{q}} = \mathbf{f}(\mathbf{q}, \dot{\mathbf{q}}, t) \Rightarrow \mathbf{M}(t)\ddot{\mathbf{q}}(t) + \mathbf{C}(t)\dot{\mathbf{q}}(t) + \mathbf{K}(t)\mathbf{q}(t) = \mathbf{f}(\mathbf{z}, t) \quad (3)$$

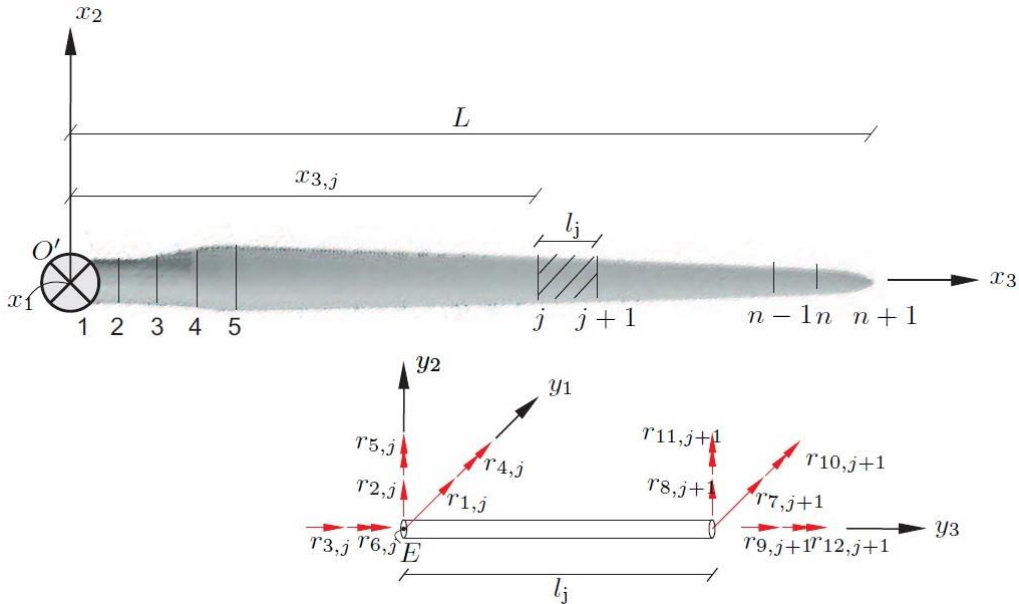


Fig. 4 Nodal numbering and definition of degrees of freedom of a beam element

Under the linear elastic deformation assumption, the mass matrix $\mathbf{M}(t)$, the damping matrix $\mathbf{C}(t)$ and the stiffness matrix $\mathbf{K}(t)$ merely depend $\mathbf{q}_0(t)$ and $\dot{\mathbf{q}}_0(t)$, and more specific on $q_6(t)$ and $\dot{q}_6(t)$. But as elaborated in Eq. (1), the $q_6(t)$ and $\dot{q}_6(t)$ can be ignored. Thus the mass matrix $\mathbf{M}(t)$, the damping matrix $\mathbf{C}(t)$ and the stiffness matrix $\mathbf{K}(t)$ all becomes periodic functions of t with the period $2\pi/\Omega$. The mass matrix $\mathbf{M}(t)$ is symmetric and positive definite, whereas the damping matrix $\mathbf{C}(t)$ and the stiffness matrix $\mathbf{K}(t)$ are nonsymmetric due to gyroscopic forces. The periodicity of the motion function can be eliminated by applying the a MBC (also known as the Coleman transformation Johnson (1980), Laks (2011)) Hansen (2004). $\mathbf{f}(\mathbf{z}, t)$ on the right hand side of Eq. (3) indicates the load vector conjugated to $\mathbf{q}(t)$ from self-induced aeroelastic loads and pitch control. Eq. (3) can be further written into a state vector form, with $\mathbf{z}(t)$ indicating the system

$$\mathbf{z}(t) = \begin{bmatrix} \mathbf{q}(t) \\ \dot{\mathbf{q}}(t) \\ \beta(t) \end{bmatrix} \quad (4)$$

The state variable $\beta(t)$ denotes a full-span collective pitch angle with a time delay determined by the first order filter

$$\dot{\beta}(t) = \frac{1}{\tau}(\beta_0(q_6, \dot{q}_6) - \beta(t)) \quad (5)$$

$\beta(t)$ is considered positive, when rotating in the positive x_3 -direction, see Fig. 3. $\beta_0(q_6, \dot{q}_6)$ indicates the pitch demand, which is modeled as PI controller with feed-back from $q_6(t)$ and $\dot{q}_6(t)$ Ogata (2010), Luo (2012). The parameter τ specifies the reaction time of the pitch actuators.

2.2 Aeroelastic load model

The boundary layers on the profile are assumed to be fully attached, and the quasi-static aerodynamic is assumed, which means a change of the angle of attack is causing a comparable change of the aerodynamic loads without time delay. Assuming locally 2D-flow around the profile the lift and drag load per unit length $p_l(x_3, t)$ and $p_d(x_3, t)$ at the position x_3 at the time t become

$$\left. \begin{aligned} p_l(x_3, t) &= c_l(\alpha) \frac{1}{2} \rho V^2(x_3, t) c(x_3) \\ p_d(x_3, t) &= c_d(\alpha) \frac{1}{2} \rho V^2(x_3, t) c(x_3) \end{aligned} \right\} \quad (6)$$

where $c_d(x_3, t)$ and $c_l(x_3, t)$ indicate the lift and drag coefficients obtained from static 2D wind tunnel test data, $\alpha(x_3, t)$ is the instantaneous angle of attack, ρ is the mass density of air, $V(x_3, t)$ is the resulting wind velocity and $c(x_3)$ is the chord length of the profile at the coordinate x_3 .

The direction of mean wind velocity V_0 is parallel to the global X_1 -direction, and is assumed to be constant over the rotor area. Further, the nominal rotational speed of the rotor Ω is also assumed to be constant in time. Hence, the resulting wind velocity $V(x_3, t)$ on the profile is given

$$V(x_3, t) = \sqrt{V_1^2(x_3, t) + V_2^2(x_3, t)} \quad (7)$$

Fig. 3 shows the wind velocities in the rotor plane. $V_1(x_3, t)$ and $V_2(x_3, t)$ are the instantaneous wind velocities in local x_1 -direction and x_2 -direction, respectively, seen by an observer fixed to the moving (x_1, x_2, x_3) -coordinate system. These are given as

$$\left. \begin{aligned} V_1(x_3, t) &= (1 - a)V_0 + v_1(x_3, t) - \dot{u}_1(x_3, t) \\ V_2(x_3, t) &= (1 + a')\Omega x_3 + v_2(x_3, t) - \dot{u}_2(x_3, t) \end{aligned} \right\} \quad (8)$$

where $a(x_3)$ and $a'(x_3)$ indicate the axial and tangential induction coefficients, obtained by BEM Hansen (2015). $v_j(x_3, t)$ indicate the components in the moving frame of reference of the rotational sampled turbulence at the position x_3 , at the time t . $\dot{u}_j(x_3, t)$ denote the corresponding moving frame components of the velocity vector of the blade at the abscissa x_3 , due to elastic deformations of the tower and the blade.

A frozen isotropic and homogeneous turbulence field is modelled using fully correlated vector ARMA model Krenk (2011), Do (2016). Based on the Taylor's hypothesis of frozen turbulence, the rotational sampled turbulence is obtained by converting the frame field into the rotor in the global X_1 -direction with a mean velocity V_0 .

The instantaneous angle of attack is given as

$$\alpha(x_3, t) = \varphi(x_3, t) + \beta(t) + \delta(x_3) \quad (9)$$

where $\varphi(x_3, t)$ indicates the flow angle defined as, see Fig. 3

$$\tan \varphi(x_3, t) = \frac{V_1(x_3, t)}{V_2(x_3, t)} \quad (10)$$

The lift coefficient $c_l(\alpha)$ and drag coefficient $c_d(\alpha)$ are calculated based on the instantaneous angle of attack together with 2D profile data. The delay effect on the loads due to change of α has not been considered here.

3. Flutter monitoring

At the onset of flutter the coupled torsional and flapwise vibrations are harmonic with the angular frequency ω_0 . Hence, the torsional vibration at the position x_3 may be written as

$$\theta(x_3, t) = \text{Re}(\Theta(x_3)e^{i\omega_0 t}) \quad (11)$$

where $\Theta(x_3)$ is the torsional flutter mode. This may be complex indicating possible phase lags along the blade. ω_0 is identified by FFT of the obtained value of the torsional angle.

The torsional vibration signal $\theta(x_3, t)$ is specified as one of the components of $\mathbf{q}(t)$ and can be obtained through an actual-torsional arithmetic unit of the structural monitoring system, which transformed the strain signals measured by a series of strain sensors mounted on both the leading edge side and the trailing edge side along the center of torsion of the blade to the real torsional angle, Ako (1992). Here, we only consider the torsional vibration signal of the blade tip $\theta(t) = \theta(L, t)$.

Due to the non-stationarity of the flutter process, the actual measurement $\theta(t)$ under flutter condition contains some lower frequency components other than the flutter mode component. Hence, in order to extract the torsional flutter mode signal, the Hilbert-Huang Transform (HHT) is applied.

$\theta_e(t)$ is defined as a envelope process of the torsional flutter mode signal that can be obtained through the Hilbert-Huang Transform (HHT), Huang (2014), Chu (2014), Yan (2014), Tang (2011). Firstly, the measured original torsional vibration signal $\theta(t)$ is decomposed into n th Intrinsic Mode Functions (IMFs) through Empirical Mode Decomposition (EMD) that each resulting IMF only has one natural frequency component, given as

$$\theta(t) = \sum_{i=1}^n c_i(t) + \varepsilon_n(t) \quad (12)$$

where $c_i(t)$ denotes the i th mode IMF, Huang (2014), $\varepsilon_n(t)$ is the residual signal at a truncation at n th mode. $c_i(t)$ can be obtained through the following process.

Firstly, based on the original signal $\theta(t)$, the upper and lower envelopes can be obtained. $m_{1,0}(t)$ indicates the mean value of the upper and lower envelopes of the original signal $\theta(t)$. The difference between the original signal and $m_{1,0}(t)$ is the first protomode, $h_{1,1}$, given

$$h_{1,1}(t) = \theta(t) - m_{1,0}(t) \quad (13)$$

Then, in order to satisfy the definition of an IMF, the Eq. (13) should be repeated as many times as is required.

After k times of iterations

$$h_{1,k}(t) = h_{1,k-1}(t) - m_{1,k-1}(t) \quad , \quad k = 2, 3, \dots, n \quad (14)$$

$m_{1,k-1}(t)$ denotes the mean value of the upper and lower envelopes of $h_{1,k-1}(t)$. the stoppage criteria Huang (2014) are satisfied, and $h_{1,k}(t)$ becomes the 1st IMF $c_1(t)$, given

$$c_1(t) = h_{1,k}(t) \quad (15)$$

The 1st IMF $c_1(t)$ should contain the finest scale or the shortest-period oscillation in the signal $\theta(t)$. The residue, $\varepsilon_1(t)$, still contains longer-period variations. This residual is then treated as the new original signal and subjected to the same sifting process as described above to obtain an IMF of lower frequency. The procedure can be repeatedly applied to all subsequent $\varepsilon_i(t)$ and the result is Huang (2008)

$$\varepsilon_1(t) = \theta(t) - c_1(t) \quad (16)$$

$$\varepsilon_{i-1}(t) - c_i(t) = \varepsilon_i(t) \quad , \quad i = 2, \dots, n \quad (17)$$

Since the frequency contents of $\theta(t)$ under flutter condition is dominated by the highest frequency component, apparently, the 1st IMF $c_1(t)$ should be chosen to represents the flutter mode signal. Finally, $\theta_e(t)$ can be obtained by calculating the amplitude of the 1st IMF $c_1(t)$ through a Hilbert Transform, given

$$\theta_e(t) = |H(c_1(t))| \quad (8)$$

where $H(\cdot)$ signified the Hilbert Transform.

The criterion of onset of flutter is taken as

$$\theta_e(t) = \theta_m$$

Here, the critical value θ_m has been set as the mean value of the time serious of torsional angle of the blade tip plus three standard deviations under the stability situation for the following reason. Let μ_θ and σ_θ indicate the mean value and the standard deviation of elastic deformations of the torsional rotation $\theta(t)$, caused by the turbulence alone. The indicated statistical moments

and determined by ergodic sampling of a suitable line series before the onset of flutter. The value of 3 standard deviations from the mean value $\theta_m = \mu_\theta + 3 \sigma_\theta$ has been chosen as a compromised to limit the probability of false alarms due to elastic exceedances of the threshold level, and to prevent structural damages at the onset of flutter.

4. Numerical example

Data from the DTU 10MW reference wind turbine Bak (2013) have been used to calibrate the structural model. The constant parameters employed in the 907-DOF wind turbine model are calculated and provided in Table 1. The frequency characteristics of the 907-DOF wind turbine model is provided in Table 2. ζ_0 and I denote the structural damping ratio and turbulence intensity, respectively.

Table 1 Parameters in the 907-DOF wind turbine model

Parameter	Value	Unit
L	89.166	m
s	5	m
h	119	m
J_r	$1.5696 \cdot 10^8$	kgm^2
J_g	2328.24	kgm^2
k_r	$3.48 \cdot 10^9$	Nm/rad
k_g	$1.392 \cdot 10^6$	Nm/rad
Ω	1.0053	rad/s
g	9.81	m/s^2
θ_m	0.045	rad
ρ	$1.0 \cdot 10^3$	kg/m^3
V_0	15	m/s
ζ_0	0.005	-
I	0.1	-

Table 2 Natural frequencies of the 907-DOF wind turbine model

Item	Value	Unit	Description
ω_f	4.15	rad/s	1st flapwise frequency of blade
ω_e	6.09	rad/s	1st edgewise frequency of blade
ω_θ	37.77	rad/s	1st torsional frequency of blade
ω_{fa}	2.75	rad/s	1st tower fore-aft frequency
ω_l	2.75	rad/s	1st tower lateral frequency

4.1 Result and discussion

Fig. 5 shows the original time series and corresponding Fourier spectrum of the torsional vibration signal of the blade tip $\theta(t)$. For the convenience of representation, only three IMFs are plotted as follow. As seen, $\theta(t)$ is mainly dominated by one frequency component (i.e., the highest frequency component).

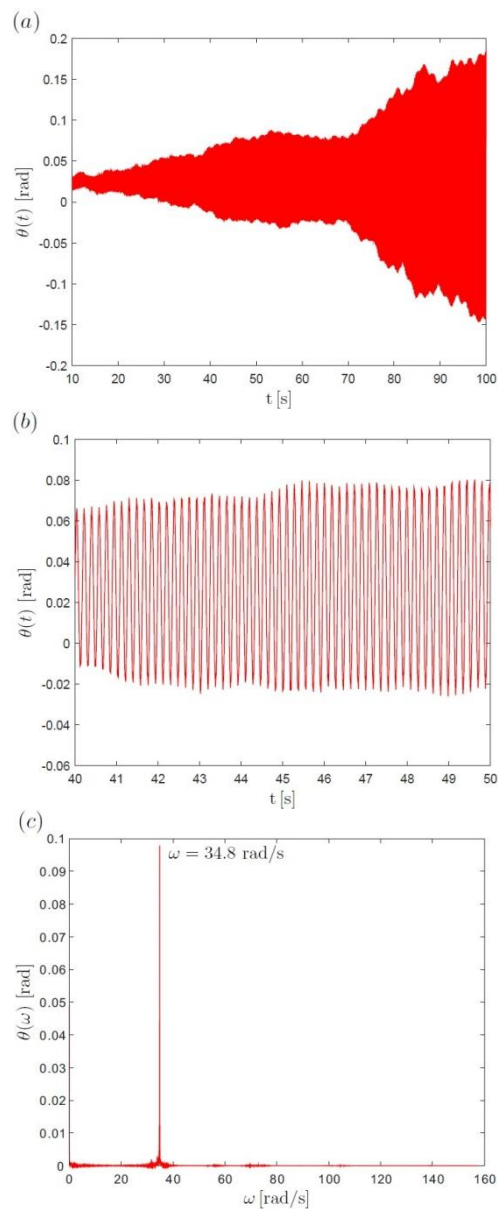


Fig. 5 Original signal and its Fourier spectrum of torsional angle of the blade tip. (a)(b) Time series of torsional angle $\theta(t)$ of the blade tip, (b) Fourier spectrum $\theta(\omega)$

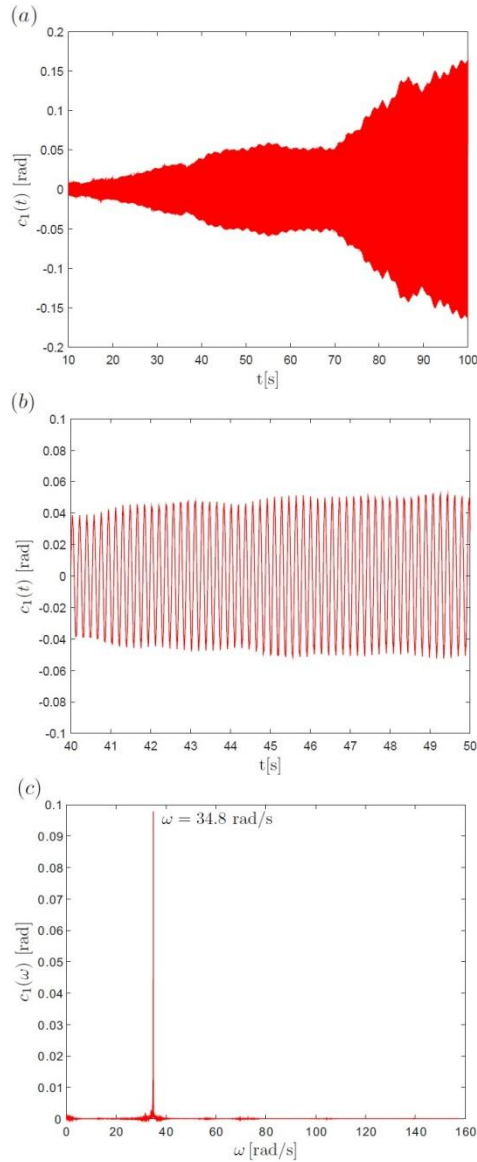


Fig. 6 IMF and Fourier spectrum of the decomposed 1st mode $c_1(t)$. (a)(b) Time series $c_1(t)$, (b) Fourier spectrum $c_1(\omega)$

Fig. 6-8 show the 1st, 2nd and 3rd IMFs of $\theta(t)$, respectively. Fig. 6(b) shows that the 1st IMF contains the same highest frequency component as the $\theta(t)$ does. Due to the lower frequency components, the mean value of $c_1(t)$ is a little bit smaller than $\theta(t)$ by comparing Figs. 5(a) and 5(b) with Figs. 6(a) and 6(b). Figs. 7(b) and 8(b) show that the 2nd and 3rd IMFs contain lower frequency components of $\theta(t)$ and their contribution is much smaller than $c_1(t)$. Apparently, 1st IMF $c_1(t)$ plays significant part in $\theta(t)$, which represents the flutter mode.

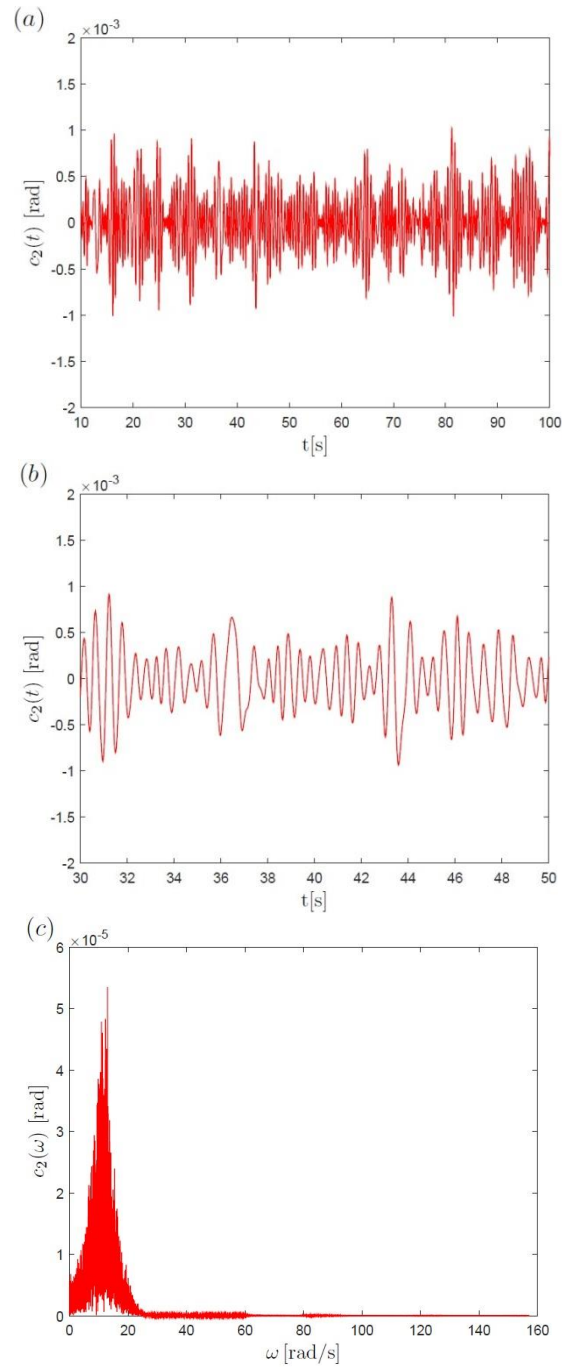


Fig. 7 IMF and Fourier spectrum of the decomposed 2nd mode $c_2(t)$. (a)(b) Time series $c_2(t)$, (b) Fourier spectrum $c_2(\omega)$

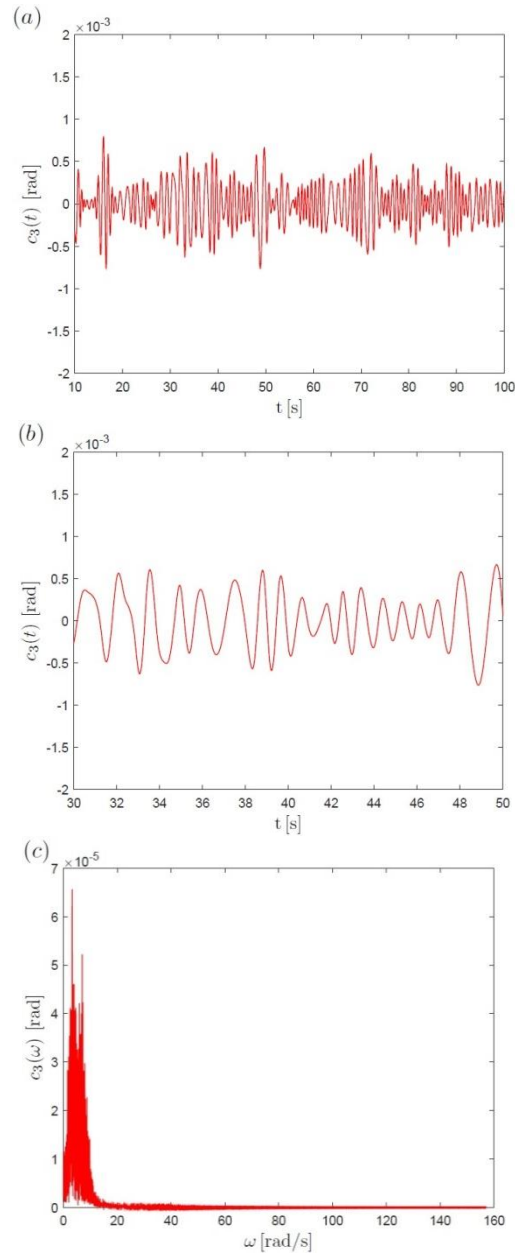


Fig. 8 IMF and Fourier spectrum of the decomposed 3rd mode $c_3(t)$. (a)(b) Time series $c_3(t)$, (b) Fourier spectrum $c_3(\omega)$

Fig. 9 shows the time series of the envelope process $\theta_e(t)$ calculated from Eq. (18). As seen, as the envelope $\theta_e(t)$ exceeds the critical value $\theta_m(t)$, the vibration starts to increase beyond limits, indicating instability.

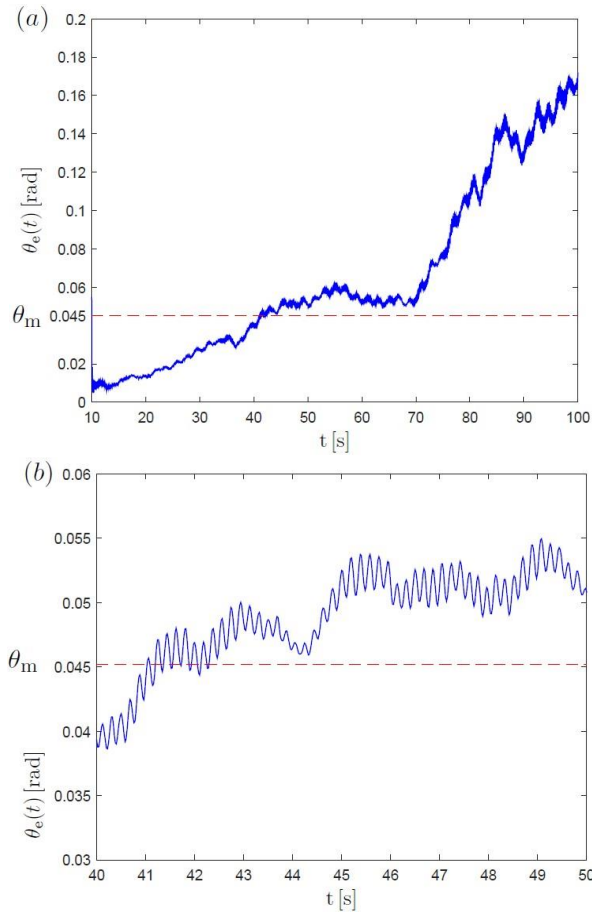


Fig. 9 Time series of envelope process $\theta_e(t)$

5. Conclusions

Motivated by the flutter monitoring problem of wind turbine blade, we have proposed an output only online approach towards fast online detecting of the flutter onset. The criterion for the onset of flutter has been described in detail. This method firstly decomposes the original torsional vibration time series of the blade tip into several IMFs. Then, the 1st IMF is chosen, which represents the flutter mode, to calculate its envelope process through the Hilbert Transform. Finally the flutter onset criterion is described. This method can be carried out online without any time delay. Further, the criterion for the onset of flutter is more practical for engineers to determine the stability of wind turbine blade merely based on the online measurements. The effectiveness and accuracy of the proposed method has been verified numerically through a 907-DOFs aeroelastic model, which is supposed to mimic the real turbine in a turbulent inflow to the rotor.

Acknowledgments

The first author gratefully acknowledges the financial support from the Chinese Scholarship Council under the State Scholarship Fund. The support of National Science Foundation of China (No. 51278189, No. 51422806) and the State's Key Project of Research and Development Plan (No. 2016YFE0127900) are also greatly acknowledged. The fourth and the fifth authors gratefully acknowledge the funding from the European Commission under the FP7 ITN project SYSWIND (Grant no. 238325).

References

- Ako, H. (1992), Flutter control system for aircraft wings, US Patent 5,135,186, Google Patents, USA.
- Bak, C., Zahle, F., Bitsche, R., Kim, T., Yde, A., Henriksen, L. C., Natarajan, A. and Hansen, M. (2013), Description of the DTU 10 MW Reference Wind Turbine 2013, DTU Wind Energy Report-I-0092, Cph, Denmark.
- Bir, G. and Jonkman, J. (2007), "Aeroelastic instabilities of large offshore and onshore wind turbines- art. no. 012069", *Science of Making Torque from Wind. Journal of Physics Conference Series*, **75**, Denmark, Lyngby, August.
- Chen, B., Zhang, Z.L., Hua, X.G., Nielsen, S.R.K. and Basu, B. (2016), "Enhancement of flutter stability in wind turbines with a new type of passive damper of torsional rotation of blades", *J. Wind Eng. Ind. Aerod.*, under review.
- Chu, P.C., Fan, C.W. and Huang, N. (2014), "Derivative-optimized empirical mode decomposition for the Hilbert–Huang transform", *J. Comput. Appl. Math.*, **259**, 57-64.
- Do, D.P.N., Lee, Y. and Choi, J. (2016), "Hourly average wind speed simulation and forecast based on ARMA model in Jeju Island, Korea", *J. Elec. Eng. Technol.*, **11**(6), 1548-1555.
- Hansen, M.H. (2004), "Aeroelastic stability analysis for for wind turbines using an eigen value approach", *Wind Energy*, **7**(2), 133-143
- Hansen, M.H. (2007), "Aeroelastic instability for wind turbines", *Wind Energy*, **10**(6), 551-577.
- Hansen, M.O.L. (2015), *Aerodynamics of Wind Turbines*, (3rd Ed.), Routledge, UK.
- Hayat, K., De Lecea, A.G.M., Moriones, C.D. and Ha, S.K. (2016), "Flutter performance of bend– twist coupled large-scale wind turbine blades", *J. Sound Vib.*, **370**, 149-162.
- Hsu, M.C., Akkerman, I. and Bazilevs, Y. (2014), "Finite element simulation of wind turbine aerodynamics: Huang, N.E. (2014), *Hilbert-Huang transform and its applications*, World Scientific, Singapore.
- Huang, N.E. and Wu, Z.H. (2008), "A review on Hilbert-Huang transform: Method and its applications to geophysical studies", *Rev. Geophysics*, **46**(2).
- Johnson, W. (1980), *Helicopter Theory*, Princeton Univ. Press, USA.
- Krenk, S. (2011), "Explicit calibration and simulation of stochastic fields by low-order ARMA processes", *Eccomas Thematic Conference-Compdyn 2011*.
- Laks, J., Pao, L., Wright, A., Kelley, N, and Jonkman, B.(2011), "The use of preview wind measurements for blade pitch control", *Mechatronics*, **21**(4), 668-681.
- Lobitz, D. W. and Veer, P. S. (1998), "Aeroelastic behavior of twist-coupled HAWT blades", *AIAA Paper*, 98-0029.
- Lobitz, D.W. (2004), "Aeroelastic stability predictions for a MW-sized blade", *Wind Energy*, **7**(3), 211-224.
- Luo, Y. and Chen, Y.Q. (2012), "Stabilizing and robust fractional order PI controller synthesis for first order plus time delay systems", *Automatica*, **48**(9), 2159-2167.
- Lurie, A. I. (2013), *Analytical mechanics*, Springer Science & Business Media Press, New York, USA.
- Mevel, L., Basseville, M. and Benveniste, A. (2005), "Fast in-flight detection of flutter onset: a statistical approach", *J. Guid. Control, Dynam.*, **28**(3), 431-438.

- Nayfeh, A.H. and Mook, D.T. (1995), *Nonlinear Oscillations*, John Wiley and Sons, New York, USA.
- Ogata, K. (2010), *Modern Control Engineering*, (5th Edition), Pearson, USA.
- Politakis, G., Haans, W. and Van Bussel, G. J. W. (2008), "Suppression of classical flutter using a 'smart blade'", *Proceedings of the 46th AIAA Aerospace Sciences Meeting and Exhibit*, Reno, USA, January.
- Popelka, D. (1982), Aeroelastic stability analysis of a Darrieus wind turbine, Sandia National Laboratories, Albuquerque, California, USA.
- Tang, J.P., Chiou, D.J., Chen, C.W., Chiang, W.L., Hsu, W.K., Chen, C.Y. and Liu, T.Y. (2011), "RETRACTED: A case study of damage detection in benchmark buildings using a Hilbert-Huang Transform-based method", *J. Vib. Control*, **17**(4), 623-636.
- Tcherniak, D. (2011), "Rotor anisotropy as a blade damage indicator for wind turbine structural health monitoring systems", *Mech. Syst. Signal Pr.*, **74**, 183-198.
- validation study using NREL Phase VI experiment", *Wind Energy*, **17**(3), 461-481.
- Vatne, S.R. (2011), "Aeroelastic instability and flutter for a 10 MW wind turbine", *Institutt for energi-og prosessteknikk*.
- Yan, J. and Lu, L. (2014), "Improved Hilbert–Huang transform based weak signal detection methodology and its application on incipient fault diagnosis and ECG signal analysis", *Signal Processing*, **98**, 74-87.
- Zhang, P. and Huang, S. (2011), "Review of aeroelasticity for wind turbine: Current status, research focus and future perspectives", *Frontiers in Energy*, **5**(4), 419-434.
- Zhang, Z.L., Nielsen, S.R.K., Blaabjerg, F. and Zhou, D. (2014), "Dynamics and control of lateral tower vibrations in offshore wind turbines by means of active generator torque", *Energies*, **7**(11), 7746-7772.
- Zhou, W. S., Maalej, S., Zouari, R., Mevel, L., De B. and IRISA-Campus (2007), "Flutter monitoring with the statistical subspace method for the 2-d structure", *Proceedings of the 25th International Modal Analysis Conference (IMAC-XXV)*, Orlando, FL, US.
- Zouari, R., Mevel, L. and Basseville, M. (2012), "Adaptive statistical approach to flutter detection", *J. Aircraft*, **49**(3), 735-748.